Journal of the Optical Society of America B
OPTICAL PHYSICS

Alternative bridging architectures in organic nonlinear optical materials: comparison of π- and χ-type structures

Meghana Rawal,[1] Kerry E. Garrett,[1] Lewis E. Johnson,[1] Werner Kaminsky,[1] Evgheni Jucov,[2] David P. Shelton,[3] Tatiana Timofeeva,[2] Bruce E. Eichinger,[1] Andreas F. Tillack,[1] Bruce H. Robinson,[1,*] Delwin L. Elder,[1] and Larry R. Dalton[1]

[1]Department of Chemistry, University of Washington, Seattle, Washington 98195, USA
[2]Department of Chemistry, New Mexico Highlands University, Las Vegas, New Mexico 87701, USA
[3]Department of Physics and Astronomy, University of Nevada, Las Vegas, Nevada 89154-4002, USA
*Corresponding author: robinson@chem.washington.edu

Received 12 August 2016; revised 28 September 2016; accepted 2 October 2016; posted 3 October 2016 (Doc. ID 273715); published 8 November 2016

Organic nonlinear optical (ONLO) chromophores are used to make electro-optic devices. Traditional ONLO chromophores use a π-conjugated bridge to couple the electron acceptor and donor moieties. We have explored whether other types of conjugation can be used to make high-performance ONLO chromophores. We have found that cross-conjugated bridge structures, when other parameters are kept the same, can exhibit comparable hyperpolarizabilities. Experimental hyperpolarizabilities of prototypical cross-conjugated chromophores, measured by hyper-Raleigh scattering, are comparable with their π-conjugated analogues, in contrast with the prediction of several electronic structure calculation methods. This opens new synthetic routes to other types of chromophores, which may provide enhanced performance.

OCIS codes: (190.4710) Optical nonlinearities in organic materials; (190.4720) Optical nonlinearities of condensed matter; (310.6805) Theory and design.

http://dx.doi.org/10.1364/JOSAB.33.00E160

1. INTRODUCTION

Organic nonlinear optical (ONLO) chromophores have recently shown themselves to be extremely efficient as the active components in Mach–Zehnder-type electro-optic (EO) modulators. The chromophores have been employed as the nonlinear optical material in silicon-organic-hybrid (SOH) [1,2] and plasmonic-organic-hybrid (POH) [3–5] devices. In such devices one important figure of merit is the electro-optic coefficient, r_{33}. A larger r_{33} results in greater sensitivity to encoding voltage into optical signals (and vice versa).

The EO coefficient depends on three parameters: the overall acentric order of the chromophores, $\langle \cos^3 \theta \rangle$, the overall number density of the chromophores, ρ_N, and the inherent hyperpolarizability of the individual chromophores, $\beta_{zzz}(-\omega; 0, \omega)$, by the following relation:

$$r_{33} = \frac{2g(\omega, \varepsilon)}{n_\omega^4} \beta_{zzz}(-\omega; 0, \omega) \rho_N \langle \cos^3 \theta \rangle. \quad (1)$$

Note that, for the systems discussed in this work, the local field factor typically is $\frac{2g(\omega,\varepsilon)}{n_\omega^4} \approx 1$, as discussed below. Most generally such organic chromophores are made as a asymmetric molecule, where on one end, the donor provides a pair of electrons into a bridging π system, and on the other end, the acceptor receives the electronic charge (Fig. 1).

One way to optimize r_{33} is to design chromophores with higher molecular hyperpolarizability. The two-level model [6] provides insight into how to recognize a molecule that gives a large β. The principle is that intra-molecular charge transfer between the electron donor on one end and the electron acceptor on the other end of the molecule causes a shift in the dipole moment from the ground state, to the first excited state, also called the charge transfer state. The difference between the ground and charge transfer state dipole moments, μ_{00} and μ_{11}, respectively, should be as large of possible, as should the transition dipole moment, μ_{10}, which is related to the oscillator strength. Also, the molecular bandgap (which is approximately the energy difference between the lowest unoccupied molecular orbital [LUMO] and the highest occupied molecular orbital [HOMO] levels of the molecule), $E_1 - E_0$, should be as small as possible. The two-level model relationship for the hyperpolarizability, β, using the Pockel's effect is

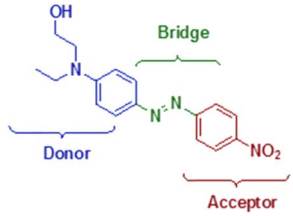

Fig. 1. Structure of disperse Red 1(DR1) chromophore.

$$\beta_{zzz}(-\omega;0,\omega)=\frac{1}{2}\frac{(\mu_{11}-\mu_{00})|\mu_{10}|^2}{(E_1-E_0-\hbar\omega)^2}. \quad (2)$$

Strong donors typically increase the energy of the HOMO, whereas strong acceptors decrease the energy of the LUMO. In either case, this leads to a reduction in the energy band gap, thereby increasing β. Indeed strong donors (e.g., arylamines and triarylamines) and strong acceptors [e.g., 2-(dicyanomethylene)-2,5-dihydro-4,5,5-trimethylfuran-3-carbonitrile (dimethyl-TCF) and 2-(dicyanomethylene)-2,5-dihydro-4-methyl-5-oxo-1H-pyrrole-3-carbonitrile (TCP)] are typically part of the structure of some of the current high β molecules that have been developed (Fig. 2).

The drawback to lowering the band gap is the bathochromic shift of the maximum absorption wavelength of the molecule. As this wavelength, λ_1, of this transition, where $\frac{hc}{\lambda_1}=E_1-E_0$, approaches telecommunication wavelengths (1310 and 1550 nm), absorptive losses within an electro-optic device become significant. Extension of the bridge, increasing the conjugation length of a polyene structure, also leads to higher hyperpolarizabilities and a bathochromic shift of the absorption maximum. An increase in bridge length, however, reduces the photo- and thermal stability of the molecule. This is overcome by using ring-locked (CLD-type) isophorone bridges [7–11], as seen in YLD-124 (Fig. 2). Heteroaromatic thienyl-vinylene bridges (FTC type) [10,12,13], as seen in YLD-156 (Fig. 2) and EZ-FTC, offer high thermal and photostability without significant loss in β along with well-established syntheses. Thiophene moieties also offer a point of substitution for further modification of the chromophore. These organic molecules can be modified not only for larger β but also better photo-, thermal, and temporal stability, reduced optical loss at

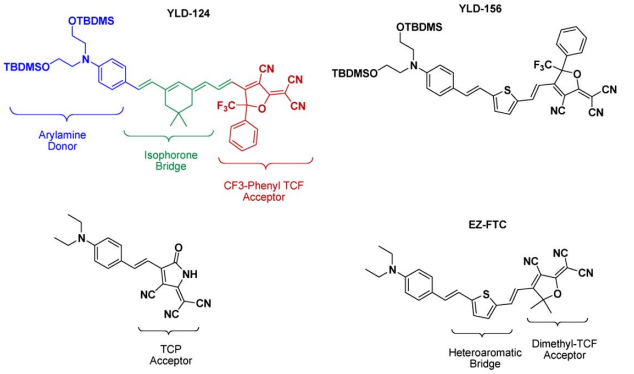

Fig. 2. Molecular structures of some important chromophores in electro-optics.

telecommunication wavelengths, and improved processability. Kuzyk *et al.* [14] have suggested a three-level model for estimating the hyperpolarizability theoretically, which requires the additional dipole moments, μ_{21} and μ_{20}, and a single additional energy parameter, E, which is the ratio of the first excited state transition to the second excited state transition, $E=\frac{E_{10}}{E_{20}}=\frac{E_1-E_0}{E_2-E_0}=\frac{\lambda_2}{\lambda_1}$. Maximum hyperpolarizability with respect to this parameter is achieved when $E=\frac{1}{2}$. Kuzyk *et al.* argue that the three-level model "is not an approximation, […] and has been shown to be true in all cases ever tested" [14]. The optical spectra provide the information needed to determine the ratio, E. Moreover, Kuzyk has developed a criterion for the maximum possible β. Therefore, comparing the β measured experimentally with the maximum value gives one a sense of how efficient the molecules are.

Having a theory that tells us to increase the change in the dipole moment for a transition with large oscillator strength does not necessarily indicate how best to construct the optimal molecule.

For a conventional chromophore, a large hyperpolarizability arises from a donor and an acceptor connected by a bridge that provides full π system conjugation. Other structures have been suggested. Some examples include X and Λ type structures [15]. Such structures generally need to form a compromise with the orientation, based on the single (effective) dipole moment, which is along the symmetry axis of the molecule. Having large off-axis components of the hyperpolarizability tensor do not translate into large electro-optic coefficients. Intra-molecularly twisted structures (TICTOID) have also been suggested, in which the π conjugation has been disrupted by a twist, $>60°$, about a single bond. Theories have suggested that the optimum hyperpolarizability will happen when there is a dihedral angle of 70°–85° [16,17]. Such structures have been shown to demonstrate some of the largest nonlinear responses to date [16,18], suggesting that alternative structures may even exceed the performance of the traditional π-conjugated motifs.

Others have suggested that one can develop a rather large dipole shift on excitation to the charge transfer state by having a disruption in the π system in the middle of the bridge. Tentative results have suggested that the experimental systems would be competitive with the traditional chromophores (shown in Fig. 2). Work on various omni-conjugated topologies by van der Veen *et al.* [19] was envisioned for use in molecular wires or switches. Studies of omni- and cross-conjugated molecules based on [3] dendralene systems produce twisted morphologies with very little electron delocalization [20,21]. Diederich and coworkers reported on the electronic characterization of a series of cross-conjugated dicyanovinyl substituted 2,3-diphenyl-1,4-butadiene derivatives. Their work indicated a quinoid character on the donor side along with efficient intramolecular CT interactions and high third-order nonlinear responses in spite of a substantial twist between the two adjacent dicyanovinyl groups [22,23]. Most of this research has suggested that the disruption needed to be carefully designed. In situations where the molecular design led to a cross conjugation without a substantial twist, spectroscopic experiments indicated large charge delocalization [24]. We have continued the study of charge transfer in cross-conjugated, $-\chi C$,

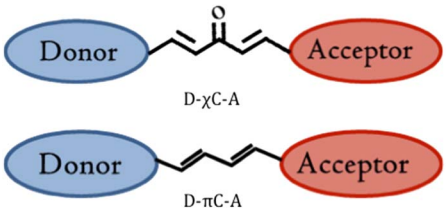

Fig. 3. Cross-conjugated, χC, design motif and corresponding in-line, or π, conjugated, πC, motif.

systems in which the interrupted π system is still kept planar to enhance overlap, and we compare cross-conjugated molecules with their fully π-conjugated, πC, analogues (see Fig. 3). Our goal is to provide an experimental basis to decide the extent to which cross conjugation can compete with the standard fully π-conjugated chromophores and further to test whether theory is able to properly simulate the relative hyperpolarizabilities measured in experiments. We note that, to the best of our knowledge, $-\chi C$ systems have not been studied for second-order nonlinear applications.

2. RESULTS (EXPERIMENTAL STUDIES)

The chromophores used in this study are shown in Fig. 4. Those collectively labeled as χC-chromophores contain a diethyl-amino benzene donor, a cross-conjugated bridge, and acceptors of varying strengths. The molecule πC-NO2 has π conjugation rather than cross-conjugation and was used as a control for direct comparison with χC-NO2. χC-NEt2 was prepared by reacting 4-diethylaminobenzaldehyde with acetone in a 2:1 molar ratio using NaOH as the base and 2-butanol as the solvent. χC-Me was made by reacting 4-diethylaminobenzaldehyde with excess acetone in the presence of aqueous NaOH. Synthesis of χC-Ph, χC-PhF, χC-CN, and χC-NO2 was achieved by condensation of χC-Me with benzaldehyde, 4-fluorobenzaldehyde, 4-cyanobenzaldehyde, and 4-nitrobenzaldehyde, respectively. πC-NO2 was prepared by heating 4-(dimethylamino)cinnamaldehyde and 4-nitrophenylacetic acid to 100°C for 3 h in the presence of piperidine. Detailed synthetic data are shown in the supporting information (as a link at the end of this paper).

To understand how the cross-conjugated analogs compare with the traditional fully conjugated systems, we examined the crystal structure of the new set of molecules in order to demonstrate the extent of planarity and similarity of the structure. Then we compared the UV/vis spectra to determine the similarity of trends with increasing solvent polarity and dielectric. We report the hyper-Raleigh scattering (HRS) based spectroscopic measurements of the hyperpolarizability. Quantum mechanical simulations were performed to predict the ground state geometries, identify the optical transitions, and compare theoretical predictions of the hyperpolarizability with experimental results.

A. Crystal Structures

Crystals were grown of compounds χC-NEt2, χC-Me, χC-CN, χC-NO2, and πC-NO2 and analyzed using x-ray diffraction. Samples of χC-Ph and χC-PhF (Fig. 4) did not yield crystals because they were viscous liquids. X-ray crystallographic data was collected at −173°C on a Bruker APEX II single crystal x-ray diffractometer, Mo-radiation. The data were integrated and scaled using SAINT, SADABS within the APEX2 software package from Bruker. An interesting feature of the χC molecules is the dihedral angle, as a twist, between the phenyl on the donor and the phenyl of the acceptor (see Fig. 5). The major contributor to the twist occurs about the carbon–carbon bond between the carbon of the ketone moiety and the neighboring carbon on the acceptor side. The twist is more pronounced on those molecules with stronger acceptors. The reference molecule, πC-NO2, does not show any twist. CCDC-1504049 (πC-NO2), 1504050 (χC-CN), 1504051

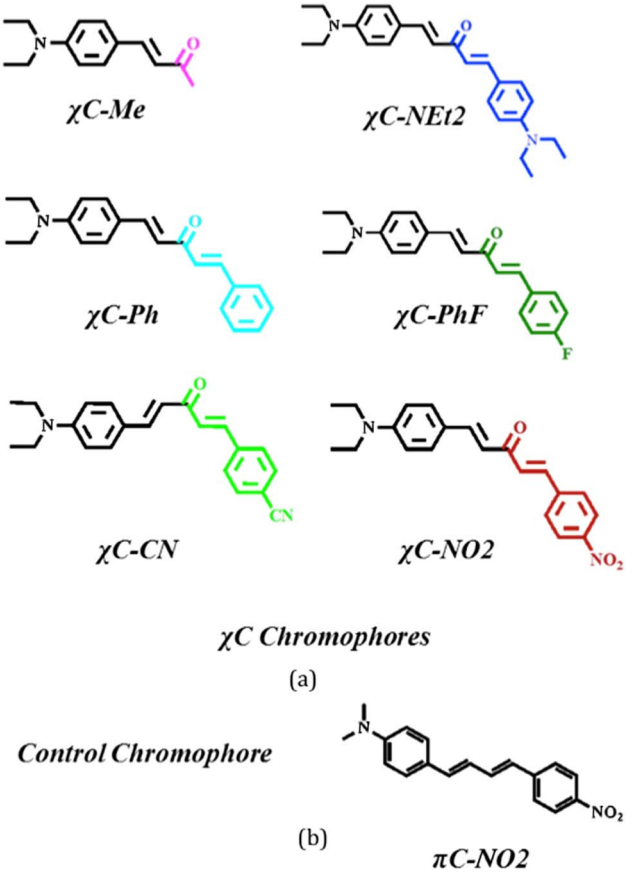

Fig. 4. (a) Structure of χC molecules cross-conjugated molecules. (b) Control for χC molecules.

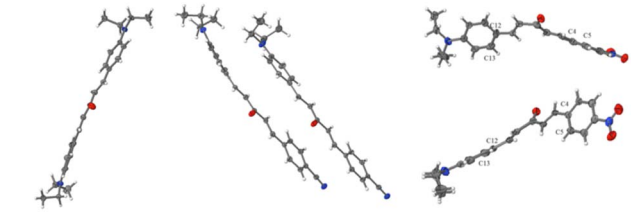

Fig. 5. Packing diagram and crystal structure showing the dihedral twist of (a) χC-Net2, (b) χC-CN, and (c) χC-NO2.

(χC-Me), 1504052 (χC-NEt), and 1504066 (χC-NO2) contain the supplementary crystallographic data for this paper. These data can be obtained free of charge from [25].

B. UV-vis Spectroscopy

The electronic properties of the χC chromophores were investigated using UV-vis spectroscopy. The spectra of each of the six molecules were obtained in a variety of solvents. To characterize the polarity of the solvents, the $E_T(30)$ scale was chosen. This scale better represents the electrostatic interactions on the solutes than solvent dielectric [26,27]; larger $E_T(30)$ values correspond to more polar solvents (with larger dielectrics). In chloroform ($E_T(30) = 39.1$ kcal/mol), χC-Me exhibits a single absorbance at 390 nm while the cross-conjugated dyes with acceptors show two $\pi \rightarrow \pi^*$ transitions (Fig. 6). The χC-NO2 is compared with πC-NO2 (Fig. 7). Both molecules show very similar low energy transitions (464 nm for χC-NO2 and 452 nm for πC-NO2). The high-energy transition (323 nm) for πC-NO2 is essentially a vibronic transition because it occurs at double the energy of the primary transition and has half the molar absorptivity.

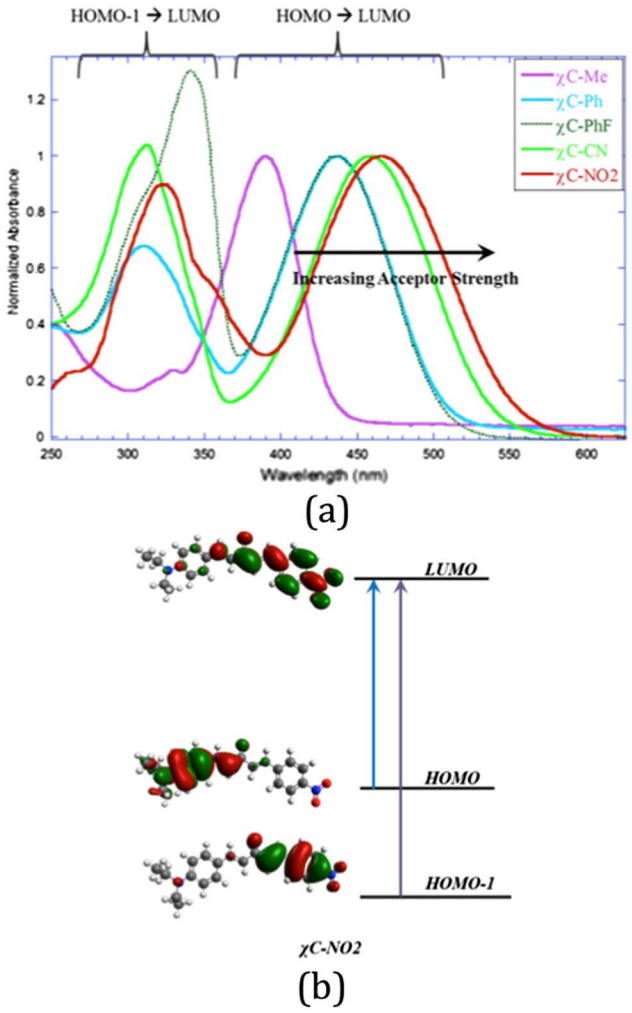

Fig. 6. (a) UV-vis spectra of cross-conjugated chromophores in chloroform. (b) Energy-level diagram from DFT simulations of χC-NO2, discussed below.

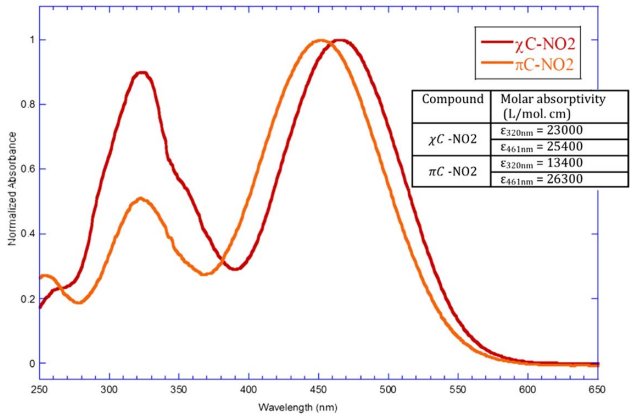

Fig. 7. UV-vis spectra of χC-NO2 versus πC-NO2 in chloroform.

The electronic properties of the chromophores were further studied by conducting a UV-vis polarity study for χC-NEt2, χC-Me, χC-CN, and χC-NO2. All of the cross-conjugated dyes show bathochromic shifts with increasing solvent polarity (Fig. 8); this is an indication of the highly polar nature of these chromophores, similar to that seen with most π-conjugated molecules. The most polar dyes χC-NEt2, χC-CN, and χC-NO2, as a group, had the largest change of the HOMO → LUMO transition in going from cyclohexane ($E_T(30) = 31$ kcal mol^{-1}) to ethanol ($E_T(30) = 52$ kcal mol^{-1}). It is interesting to note that χC-NEt2 has a much smaller net dipole than the other two in this group but a similar solvent shift; this will be discussed after Fig. 14.

C. Hyper-Rayleigh Scattering Experiments

The β values (shown in Table 1) for the chromophores in a CDCl3 solution were determined from HRS measurements at a laser wavelength of 1064 nm (using a pulsed Nd:YAG laser) and sample temperature 25°C. Calibration of the HRS results used 4-nitroaniline (pNA) in CD Cl_3 solution as a reference standard. Dilute solutions of pNA (36.4 mM), χC-NO2 (38.4 μM) and χC-NO2 (43 μM) in CDCl3 were freshly prepared for each measurement. The solution concentrations

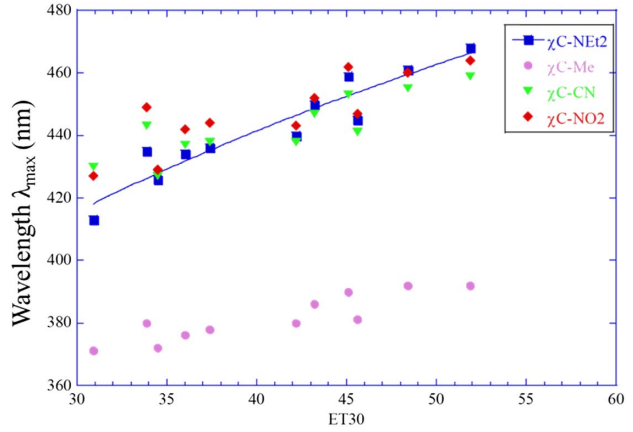

Fig. 8. UV-vis solvatochromism in the χC chromophores. Line is shown only to guide the eye.

Table 1. Experimental Hyperpolarizability Values for χC-NO2 and πC-NO2 Measured at 1064 nm, $\beta_{HRS}(-2\omega;\omega,\omega)$ and Extrapolated to Zero Frequency, $\beta_{HRS}(0;0,0)$

Molecule	$\beta_{HRS}(-2\omega;\omega,\omega)$@1064	$\beta_{HRS}(0;0,0)$
pNA	11.4 ± 1	5.9 ± 0.5
χC-NO2	479 ± 48	97 ± 10
πC-NO2	561 ± 56	132 ± 13

were chosen to give comparable signals for the chromophore and reference solutions, and the much smaller HRS signal measured for the neat solvent was subtracted. Sample and reference HRS signals were compared using the same laser focusing, collection optics, and polarization configuration, using apparatus and techniques as previously described [28,29]. The laser power incident on the sample was adjusted without affecting the alignment or focusing of the laser beam using a half-wave plate and polarizer combination.

The 532 nm (second harmonic wavelength) HRS light is absorbed by the sample along the 1.5 mm path from the laser focus to the exit window of the cuvette. The self-absorption correction was determined using the 532 nm absorbance measured for the sample in the 10 mm sample cuvette. The HRS signal at 532 nm selected by the 60 cm^{-1} bandpass filter may be contaminated with two-photon fluorescence (2PF). The fraction of the total signal due to HRS is determined from a spectral scan, where the HRS and 2PF appear as a sharp peak and a broad background, respectively. The directly measured 2PF fractions for χC-NO2 and πC-NO2 are 65% and 54%, respectively.

HRS signal S is measured versus laser power P, and S/P^2 is extrapolated to $P = 0$. This extrapolation is necessary because weak absorption of the focused laser beam in the sample heats the sample along the beam path, defocuses the beam, and reduces the HRS signal. In the absence of this thermal lens effect S/P^2 is independent of P. In the usual case of weak linear absorption by the sample at the laser wavelength, the extrapolation is done by fitting $S/P^2 = A(1 - B \times P)$ to the data (see Fig. 9).

The power-normalized HRS signal S/P^2 was independent of laser beam power P for the pNA reference solution, as expected, but S/P^2 for both chromophore solutions exhibited a strong dependence on P. For χC-NO2 and πC-NO2 there is a strong thermal lens effect that appears to be dominated by two-photon absorption, so the appropriate extrapolation function is $S/P^2 = A(1 - B \times P^2)$ instead. For these two molecules significant thermal lensing by linear absorption at 1064 nm is ruled out by direct measurements of the linear absorption at 1064 nm and by measurement of the continuous wave thermal lens effect at the same average laser power.

The experimental static hyperpolarizabilities, $\beta_{HRS(0)}$, were obtained by extrapolating from the frequency-dependent hyperpolarizabilities, $\beta(-2\omega;\omega,\omega)$ at 1064 nm ($\omega = 1.16$ eV), individually for all three samples applying the three-term frequency correction factor developed by Kuzyk (extended from the two-level model [TLM] equation of Oudar and Chemla), which contains a linewidth or damping term. The damping

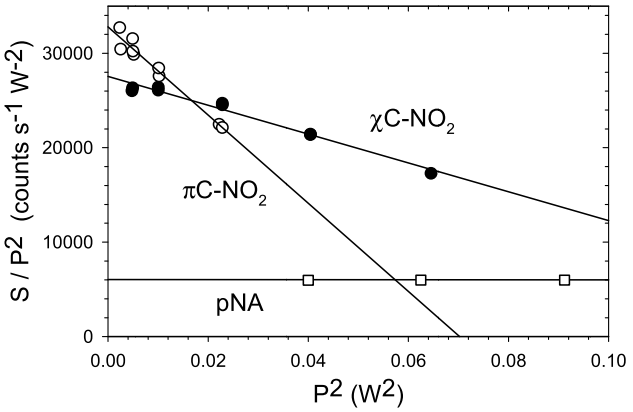

Fig. 9. Pump power dependence for hyper-Rayleigh scattering signals, showing the thermal lens effect. Symbols are data for S/P^2, and the lines fit to the data are extrapolated to $P = 0$.

term was needed because the output light at 532 nm was near the optical resonance of the samples. The damping factor $\Delta\omega$ was set to 0.1 eV, chosen so to match the homogeneous linewidth of the experimental spectra [6,30]:

$$\beta(-2\omega;\omega,\omega) = |\mathrm{cf}| \cdot \beta(0;0,0). \tag{3}$$

The correction factor, cf, depends on the ratio, R, of the frequency of the light and the resonance frequency of the sample. $R = \frac{\omega}{\omega_{max}} = \frac{\lambda_{max}}{\lambda}$, and the damping term $\gamma = \frac{\Delta\omega \cdot R}{\omega} = \frac{\Delta\omega}{\omega_{max}}$. The correction factor then is

$$\mathrm{cf} = \frac{1}{3}\left\{\frac{1}{(1 + i\gamma + 2R)(1 + i\gamma + R)} + \frac{1}{(1 - i\gamma - 2R)(1 - i\gamma - R)} + \frac{1}{(1 + i\gamma + R)(1 - i\gamma - R)}\right\}. \tag{4}$$

For χC-NO2, the ratio, $R \sim 0.436$, and the ratio damping factor, $\gamma \sim 0.0374$, lead to a correction factor $|\mathrm{cf}| \sim 4.94$, whereas, for πC-NO2 the ratio, $R \sim 0.424$, and the ratio damping factor, $\gamma \sim 0.0364$, give $|\mathrm{cf}| \sim 4.25$.

D. Cyclic Voltammetry

Cyclic voltammetry data were obtained using an 1×10^{-3} M solution of chromophore in CH_3CN, 0.1 M Bu_4NPF_6 in CH_3CN supporting electrolytes, glassy carbon working electrodes, and platinum counter-electrodes. All potentials are referenced to the Ag/Ag^+ (0.01M $AgNO_3$, 0.1M Bu_4NPF_6, CH_3CN) reference electrode. In addition, Ferrocene was used as a reference standard for energy level calculations. Cyclic voltammetry experiments were done to assess and compare the quantum mechanical calculations of the relevant Kohn–Sham molecular orbitals. Figure 10 shows the HOMO and LUMO levels from the cyclic voltammetry studies; the results support the notion that, as the acceptor strength increases, the LUMO level decreases (causing the redshift for stronger donors) while the HOMO level remains essentially unchanged.

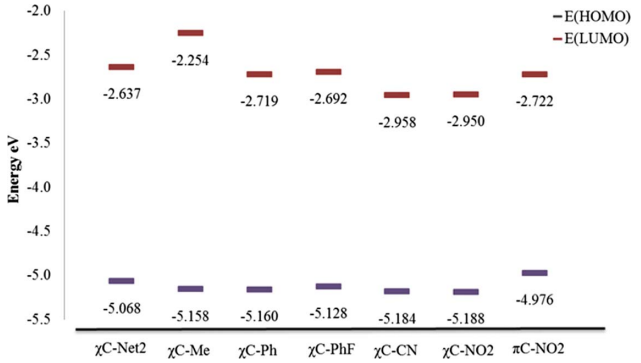

Fig. 10. HOMO–LUMO of cross-conjugated chromophores and reference chromophore measured using cyclic voltammetry.

E. Theoretical Studies Using DFT and TDDFT

The Gaussian 09 (Revision D.01) suite of QM codes [31] was used to calculate optimized geometries using the B3LYP hybrid functional [32] and the 6-31+G* basis set. These geometries were further used to calculate the molecular properties. Quantum calculations were performed using three levels of theory: (1) global hybrid density functionals (B3LYP, PBE0 [33], and M06-2x [34]), which replace a portion of the semi-local GGA exchange with Hartree–Fock (HF) exchange in order to correct for the asymptotic decay of the exchange potential at the long range; B3LYP includes a 19% HF exchange split with LYP exchange, and PBE0 uses 25% HF exchange and 75% PBE exchange contributions by 25% and 75%; the meta-GGA method M06-2 × uses a 54% HF exchange; (2) range-separated hybrid DFT (CAM-B3LYP [35]), which varies the amount of HF exchange from 19% at short range to 65% at long range; and (3) second-order Møller–Plesset perturbation theory (MP2), a computationally feasible correlated wave function method that was used for comparison with DFT.

MP2 hyperpolarizabilities were calculated at zero frequency, $\beta(0;0,0)$, by numerical differentiation of the dipole moment with respect to applied finite electric fields; frequency dependence was incorporated by calculating correction factors using Eq. (4). The theoretical absorption wavelengths (λ_{max}), used in the Eq. (4) were calculated using CAM-B3LYP/6-31 + G*. Additionally, for comparison with the two-state model, frequency-dependent DFT hyperpolarizabilities, $\beta(2\omega;\omega,\omega)$, were calculated at 1064 nm using the coupled-perturbed Kohn–Sham method with the B3LYP, PBE0, CAM-B3LYP, and M06-2 × functionals. All of the above methods incorporated solvent effects via a polarizable continuum model.

DFT calculations were used to evaluate the effects of structural changes on the molecular orbitals involved in the two lowest-energy significant optical transitions (see Fig. 6). Figures 11 and 12 show the Kohn–Sham molecular orbitals for the levels that contribute to the optical transitions evaluated using the CAM-B3LYP functional. Figure 11, bottom, illustrates that, as the strength of the acceptor increases (χC-Ph → χC-PhF → χC-CN), the electron density increases on the acceptor side, as seen in the LUMO orbital picture and is more isolated from the donor. From the analysis of the oscillator

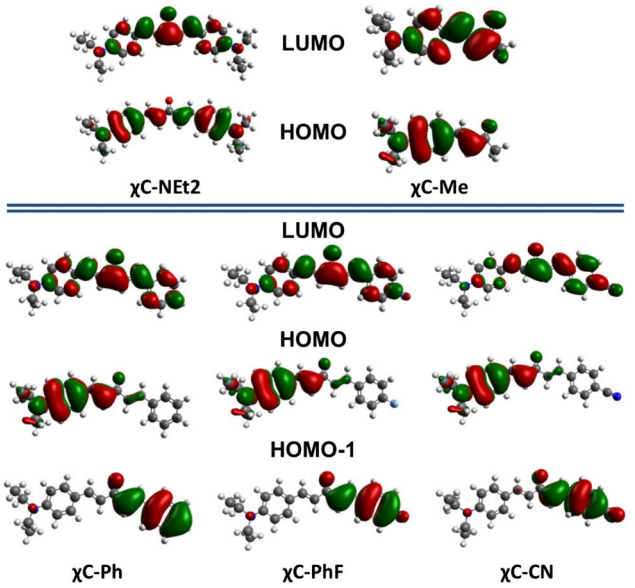

Fig. 11. Molecular orbitals for χC-NEt2, χC-Me, χC-Ph, χC-PhF, and χC-CN chromophores. MOs shown were computed at the CAM-B3LYP/6-31 + G* level of theory.

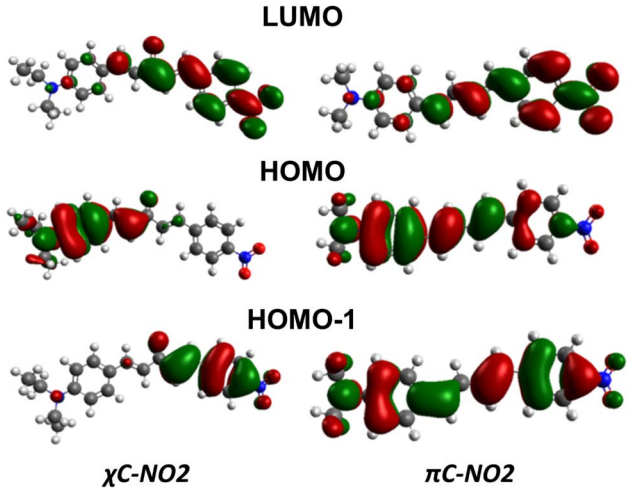

Fig. 12. Molecular orbitals for χC-NO2 and πC-NO2 chromophores. MOs shown were computed at the CAM-B3LYP/6-31 + G* level of theory.

strengths (or the transition matrix elements), one can determine that the primary optical transitions arise from the HOMO to LUMO (for the long wavelength transition) and the HOMO-1 to LUMO for the second (shorter wavelength) optical transition. According to the TD-CAM-B3LYP, the HOMO to LUMO contribution to the long wavelength (and largest oscillator strength) transition is at least 80% based on the computed CI coefficients for χC-Ph, χC-PhF, and χC-CN, which is also the case for the HOMO-1 to LUMO contribution for the second optical transition. Less significant single particle contributions arise from HOMO to LUMO+1, HOMO-2 to LUMO, etc. Figure 13 compares computed

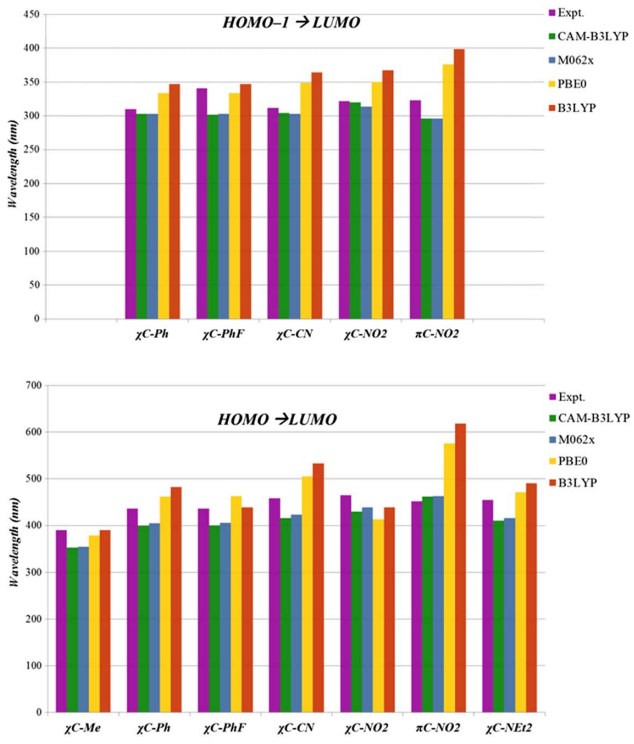

Fig. 13. Comparisons of trends in experimental and theoretical optical transitions.

optical transition wavelengths for the first two optical transitions among the different methods used and with the experimental values. The agreement is remarkably good, particularly for hybrid functionals containing more than 50% long-range Hartree–Fock exchange (CAM-B3LYP and M06-2X), which predict the primary intramolecular charge-transfer transition within 15% of measured values. Results were well-converged with respect to basis set, with results for the larger aug-cc-pVTZ basis set for χC-NO2 and πC-NO2 within 5 nm of the smaller 6-31+G* basis set.

A comparison of the experimental solvatochromic properties (shown in Fig. 8) against the theoretically calculated (CAM-B3LYP/6-31 + G*) dielectric dependence of λ_{max} (Fig. 14) shows the calculations also reflect the bathochromic trend

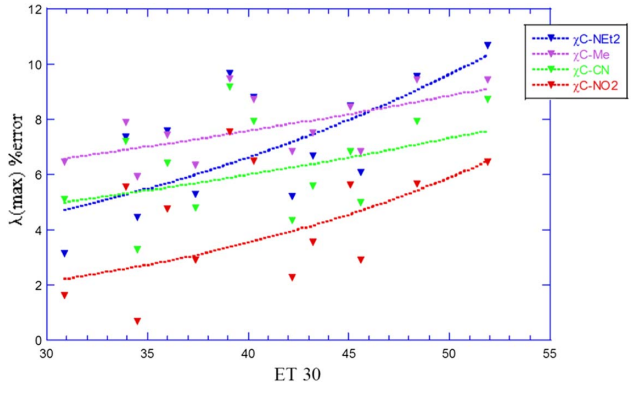

Fig. 14. Percentage error in calculation of λ_{max} using CAM-B3LYP functional with 6-31 + G* basis set. Lines are shown to guide the eye.

Table 2. Experimental (for χC-NO2 and πC-NO2) and Calculated Frequency-Dependent βHRS/βpNA Values at 1064 nm for χC Chromophores [29,36][a]

	$\beta(-2\omega,\omega,\omega)/\beta(-2\omega,\omega,\omega)$pNA					
Molecule	Expt.	B3LYP	CAM-B3LYP	M062X	PBE0	MP2
χC-Me		4.58	3.67	4.15	4.54	3.90
χC-Ph		45.41	11.08	13.59	31.60	18.70
χC-PhF		47.05	11.36	13.88	32.28	19.43
χC-CN		[b]	16.40	20.71	131.81	67.09
χC-NO2	42.0 ± 1	63.68	22.94	29.20	107.67	42.77
πC-NO2	49.2 ± 1	105.66	64.56	73.40	192.28	75.53

[a]Experimental $\beta_{pNA(1064)} = 11.4 \times 10^{-30}$ esu.
[b]On-resonance; computed $\beta(-2\omega,\omega,\omega)/\beta(-2\omega,\omega,\omega)$pNA~$3275\times10^{-30}$ esu.

observed in the experimental data albeit less accurately as the polarity of the solvent increases. The calculated absorption maximum has a somewhat weaker dependence on the dielectric than the experimental quantities.

Further theoretical simulations of molecular hyperpolarizability were performed using the four different methods described above. Table 2 shows the values for the frequency dependent HRS hyperpolarizabilities, β_{HRS}, relative to the quantity for pNA for its own experiment or calculation. The experiments and each calculation method produces different values of β_{pNA}; and each ratio is compared with the pNA value for that particular experiment or calculation. The experimental values are found in Table 1.

The experimental hyperpolarizability for πC-NO2 is about 17% larger than that for χC-NO2, and the error in the ratio is 15%. All four of the theoretical methods used predict that the cross conjugation in χC-NO2 should reduce the hyperpolarizability at 1064 nm by around a factor of two compared with πC-NO2. This prediction is in contrast with experimental results, in which the hyperpolarizabilities of χC-NO2 and πC-NO2 are within 15% of each other. The disagreement between experimental and calculated results was less dramatic after extrapolation to zero frequency (Table 1) but still significant, with a πC-NO2/χC-NO2 ratio of 1.76 at the MP2 level versus 1.38 for experiment. Results were not improved by using the larger aug-cc-pVDZ basis set for MP2 calculations; the ratio for a variant πC-NO2 with the same diethylamino donor as the cross-conjugated molecules and χC-NO2 was 1.91 using the larger basis set.

The hyperpolarizability, $\beta(-2\omega, \omega, \omega)$, for χC-NO2 was calculated at 1064 nm using the CAM-B3LYP functional but now using the twist angle constraint given by the crystallography (Fig. 5). The value of the ratio of hyperpolarizabilities, $\beta(-2\omega, \omega, \omega)/\beta(-2\omega, \omega, \omega)$pNA, calculated for a twisted χC-NO2 was 11.4. This calculated ratio is a further factor of 2 lower than that assuming the planar geometry (in Table 2), which was the optimal geometry determined using B3LYP/6-31 + G*.

F. Statistical Mechanics Calculations

Monte Carlo (MC) simulation methods have been used to simulate the density and order of an χC-NO2 and πC-NO2

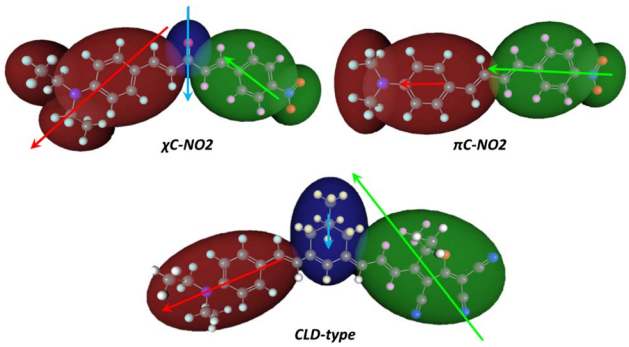

Fig. 15. Individual dipole moment contributions (identical scale for all) to donor (red arrow) and acceptor-side moieties (green arrow) alongside LoD representations used for χC-NO2 (six ellipsoids) and πC-NO2 (four ellipsoids) simulations as well as LoD representation of CLD-1 type chromophore; blue arrows indicate dipole moment contributions of cross-conjugated moiety (χC-NO2) and, for comparison, dipole moment contribution of conjugated unit in fully conjugated isophorone bridge unit of CLD-type chromophores.

system. Simulations of 108 chromophores under poling conditions at a poling field of 100 V/μm and a poling temperature of 400 K at 1 atm were performed using the isothermal isobaric ensemble (NPT) and a method to accelerate equilibrium convergence, AVA [37]. The initial, all-atom geometry and charge distribution of each chromophore is determined at the B3LYP/6-31G(d) level of theory. The molecules are then coarse-grained by replacing sections of the chromophores by ellipsoids that take into account the Lennard–Jones (LJ) pairwise interactions. This approach is called the level-of-detail (LoD) model [38].

Figure 15 shows coarse-grained representations of χC-NO2 and πC-NO2 as well as a CLD-type chromophore for comparison of the internal dipole moment contributions. Atomic partial charges (within each ellipsoid) are reduced according to the multipole expansion rules about the center of each ellipsoid (which generally consists of a dipole moment and any excess charges that may be included in each ellipsoid). We have demonstrated, elsewhere, that such an expansion well represents the intermolecular interactions of the AA force field underlying it [37,38].

The general structure of the internal dipolar distribution is remarkably similar among all three chromophores. The bent feature of the CLD-type chromophore is seen in χC-NO2 but not the πC-NO2 chromophore. The major difference is that the χC-NO2 system has a large dipole confined to the donor side, relative to the other two molecules.

In order to gain insight into the expected efficiencies of cross-conjugated molecules, we start with Kuzyk's estimate for the off-resonance maximum hyperpolarizability and the intrinsic hyperpolarizability [14]:

$$\beta_{\max} = \sqrt[4]{3}\left(\frac{e\hbar}{\sqrt{m_e}}\right)^3 N^{3/2}\frac{\lambda_{10}^{7/2}}{(hc)^{7/2}} \quad \text{and}$$
$$\beta_{\text{int}} = \frac{\beta_{zzz}(0)}{\beta_{\max}}. \tag{5}$$

The results of this calculation are shown in Table 3 along with the necessary values to compute both quantities. Note that the

Table 3. Key Figures of Merit for χC-NO2 and πC-NO2: $\beta_{\max}$ and β_{int}

Molecule	$\beta_{zzz}(0)$	λ_{10} [nm]	N	$\beta_{\max}$	β_{int} [%]
χC-NO2	234 ± 24	465	20	3451	7 ± 1
πC-NO2	318 ± 31	452	18	2669	12 ± 1

values for the static Pockels' effect hyperpolarizability, $\beta_{zzz}(0)$, were obtained from the HRS values reported in Table 1 by multiplying with $\sqrt{35/6} = 2.41$ to account for rotational averaging in the HRS experiment, and assuming that other tensor elements are insignificant [39]. Based on the measured values, the error in the hyperpolarizability was estimated to be at least 10%. The number of effective electrons is N. Here, for the types of chromophores considered, the π-conjugated electrons (two per conjugated double bond and a contributing lone pair) are the effective electrons [40].

Device performance is typically measured at an operating wavelength, ω. In order to account for this, we use the Pockel's effect frequency dispersion term from Tripathy *et al.* [40]:

$$D_\omega = \frac{\omega_0^2}{3}\left[\frac{1}{(\omega_0+i\Gamma-\omega)^2} + \frac{1}{(\omega_0+i\Gamma)(\omega_0-i\Gamma+\omega)} + \frac{1}{(\omega_0-i\Gamma)(\omega_0-i\Gamma-\omega)}\right]. \tag{6}$$

Here ω_0 is the frequency of the HOMO–LUMO transition, determined from $\lambda_{\max}$; ω is the frequency of interest, in our case $\frac{1240\frac{\text{eV}}{\text{nm}}}{1310\text{ nm}} = 0.95$ eV; and $\Gamma = 0.1$ eV is the damping factor. With this dispersion term, one can obtain the frequency-dependent hyperpolarizability as $\beta_{zzz}(\omega) = D_\omega\beta_{zzz}(0)$.

The figure of merit for EO devices is the electro-optic activity. Tillack and Robinson applied Kuzyk's concepts to define a maximum electro-optic activity, which only depends on the experimentally measurable longest wavelength optical transition, $\lambda_{\max}$ [41]:

$$r_{\max}^0 = \frac{\sqrt[4]{3}e^3}{2\varepsilon_0(hc)^2}\lambda_{\max}^2 = 7.746\cdot 10^{-3}\cdot\left(\frac{\lambda_{\max}}{\text{nm}}\right)^2\frac{pm}{V}. \tag{7}$$

In conjunction with the Pockels' effect frequency dispersion term, D_ω, the maximum electro-optic activity, at the frequency of interest, and the electro-optic efficiency are calculated as

$$r_{\max}(\omega) = D_\omega r_{\max}^0 \quad \text{and} \quad r_{\text{efficiency}} = \frac{r_{33}}{r_{\max}(\omega)}. \tag{8}$$

Table 4 presents calculation results for χC-NO2 and πC-NO2 up to this point using Eqs. (6)–(8). The electro-optic activity, r_{33}^{calc}, necessary to evaluate $r_{\text{efficiency}}$, is calculated from the

Table 4. Key Figures of Merit for χC-NO2 and πC-NO2 Calculated from Simulation Results in Table 3 at 1310 nm and a Poling Field of 100 V/μm: $r_{\max}(\omega)$ and $r_{\text{efficiency}}$[a]

Molecule	$2\frac{g(\omega)}{n_\omega^4}$	D_ω	$\beta_{zzz}(\omega)$ [10^{-30} esu]	$r_{\max}(\omega)$ [pm/V]	$r_{\text{efficiency}}$ [%]
χC-NO2	1.20	1.55	363 ± 40	1675	1.43 ± 0.42
πC-NO2	1.20	1.52	483 ± 50	1583	3.10 ± 0.69

[a]Refractive indices are assumed as $n_0 = n_\omega = 1.7$ and dielectric as that of chloroform, $\varepsilon = 4.8$.

Table 5. Results Averaged from 16 Separate Simulations for Each Molecular System under Poling Conditions at a Poling Field of 100 V/μm and a Poling Temperature of 400 K at 1 atm for χC-NO2 and πC-NO2

Molecule	$\rho[\frac{g}{cc}]$	ρ_N $[10^{20}\frac{\text{molec.}}{cc}]$	$\cos^3\theta$	r_{33}^{calc} $[\frac{pm}{V}]$	$r_{\text{intrinsic}}$ [%]
χC-NO2	0.85 ± 0.01	14.7 ± 0.1	0.09 ± 0.03	24 ± 7	16 ± 5
πC-NO2	0.82 ± 0.01	16.8 ± 0.1	0.12 ± 0.03	49 ± 11	26 ± 5

number density, ρ_N, average acentric order, $\langle\cos^3\theta\rangle$, and the frequency-dependent first-order hyperpolarizability, $\beta_{zzz}(\omega)$:

$$r_{33}^{\text{calc}} = 0.042 \cdot 2\frac{g(\omega,\varepsilon)}{n_\omega^4}\frac{\rho_N\cos^3\theta}{(10^{20}\text{ molecules/cc})}\frac{\beta_{zzz}(\omega)}{10^{-30}\text{ esu}}\cdot\frac{pm}{V}. \quad (9)$$

The electro-optic activity values for χC-NO2 and πC-NO2 calculated from the simulation results are listed in Table 5. Furthermore, by using the average acentric order of the simulated systems, as outlined in Tillack and Robinson's work, the intrinsic electro-optic activity found in Table 5 can be defined [41]:

$$r_{\text{intrinsic}} = \frac{r_{33}^{\text{calc}}}{r_{\max}(\omega)\cdot\langle\cos^3\theta\rangle}. \quad (10)$$

The electro-optic activities calculated from the simulation results for both systems are 21 ± 5 and $40 \pm 9\frac{\text{pm}}{\text{V}}$ for χC-NO2 and πC-NO2, respectively. This decrease in the electro-optic activity by nearly a factor of 2 exhibited by the cross-conjugated chromophore system compared with the conjugated one is stronger than would be expected from the reported difference of about 30% in hyperpolarizabilities found in Table 4. As can be seen in Table 5, the additional reduction is due to the decrease of both the number density, ρ_N, as well as the average acentric order, $\cos^3\theta$, of the χC-NO2 system compared with the πC-NO2 system.

The cross-conjugated molecule in this work is a proof-of-concept; it has not yet been optimized for acentric order. Due to its unique (very similar to the CLD-type chromophore) charge/dipole distribution, it is likely that design strategies found to optimize CLD-type systems [41] can be applied to a cross-conjugated system as well.

Figure 16 shows representative simulation snapshots (top) and spatial distribution functions for the acceptor nitrogen location relative to the donor nitrogen (bottom) for the χC-NO2 and πC-NO2 systems. The average acentric order in both snapshots is in the 10% range (9% and 11% for the χC-NO2 and πC-NO2 snapshots, respectively), and some chromophore stacking can be observed.

The spatial distributions functions of the acceptor nitrogen locations around the donor show differences between both chromophores. For the cross-conjugated system, the most likely acceptor locations (green areas) are close to the donor and close to the break in conjugation, around the C = O moiety. Conversely, for the straight, conjugated system with no break in conjugation, the most likely acceptor location (green areas) is around the donor with only a low likelihood (magenta areas) in the center of the molecule. Interestingly, chromophore

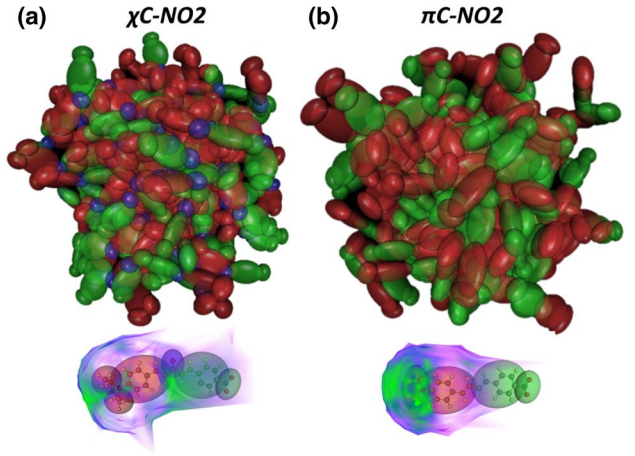

Fig. 16. Simulation snapshots (top) and spatial distribution function (bottom) of acceptor nitrogen position with respect to donor nitrogen (magenta to blue to green represent increased likelihood) of (a) χC-NO2 and (b) πC-NO2 systems.

stacking with chromophores offset by the magic angle—with the most likely acceptor region at the center of neighboring chromophores such as observed in the cross-conjugated molecule but not the conjugated one—could lead to energetically favorable, large acentric order dipolar alignment. Unfortunately, magic angle stacking also requires near parallel dipole alignment, which is not observed to a strong degree in either chromophore system. The observed behavior of the cross-conjugated system, however, once properly optimized, could be employed to maximize chromophore loading.

3. DISCUSSION/CONCLUSIONS

Our experimental and theoretical results indicate that the cross-conjugated molecules should perform nearly as well as their fully conjugated analogues. Experimentally, the optical spectra and the electrochemical data both confirm that the πC-NO2 and χC-NO2 should have similar hyperpolarizabilities. The maximum transition for χC-NO2 is actually larger than that for πC-NO2. The band gaps are nearly the same, and the hyperpolarizabilities are nearly the same (to within experimental error) in the direct measurement of the hyperpolarizability using HRS spectroscopy.

All the experimental similarities suggest that the bridges in both systems are planar in solution. The corollary is that the large twisting angles seen in the crystal structures are a result of crystal packing forces and a low energy barrier to twisting. Calculations on twisted forms of the χC molecules gave reduced values of the hyperpolarizability, suggesting that the molecules are planar in solution, and there is a small energy barrier to rotation.

The two-state model and detailed calculations suggest that the χC molecules should have about half the hyperpolarizability of the control, which is in contrast with the experimental results. The two-state model suggests that the improved dipole difference is offset by a smaller transition dipole moment (or oscillator strength). Comparison of HOMO and LUMO levels confirm this. However, the optical transitions are nearly

as strong as the control molecules. The three-state model has an additional energy ratio, E, which is 0.5 when the hyperpolarizability is optimal [14]. The strong oscillator strength of these two lowest optical transitions and the experimental energy ratio of around 0.65 also suggest that these molecules are similar to the control.

Theory, particularly both CAM-B3LYP and MO62X functionals, computes the optical transition for πC-NO2 quite accurately but predicts a larger-than-experimental band gap for the χC molecules; hence the calculated absorbance values are blueshifted by 26–42 nm, relative to the experimental values, which is one factor contributing to the underestimation of the dynamic hyperpolarizabilities of the χC molecules. DFT calculations also indicate an increasing localization of the LUMO on to the acceptor with increasing acceptor strength resulting in weak ground state molecular orbital overlap in χC-NO2 compared with the control chromophore πC-NO2 where the orbitals are much more delocalized and thus overlap significantly. This suggests that direct orbital overlap through the bridging region may not be required to obtain a substantial hyperpolarizability, in contrast with the πC-NO2 molecule, which is representative of the behavior of πC systems with acceptors consisting of a single electron-withdrawing functional group.

The dipolar features of the cross-conjugated well mimic those of the control molecules, as seen in Fig. 15. This suggests that these molecules will behave under poling in similar ways to the control groups. The simulation of the poling order predicts that the EO coefficient will be about half that of the control molecules. Notice that the CLD-type chromophore and the related chromophores (in Fig. 2) have been optimized with pendant groups to have improved order. Similar modifications to the χC molecules would be expected to give similar order enhancement. The bent structure of χC-NO2 parallels that of CLD-type chromophores; it has been shown that this bending reduces the net order in such systems [41].

This set of chromophores provide a proof of concept that cross-conjugated molecules can have hyperpolarizabilities comparable with fully conjugated molecules, at least within the range of donor and acceptor strengths examined. Whether the similarities between the cross-conjugated and the fully conjugated molecules will continue when larger chromophores with stronger acceptors are made remains an open question. However, these tentative results open up avenues for new synthetic strategies that allow for multiple donors to one acceptor or multiple acceptors to one donor mimicking star-shaped molecules suggested by Kuzyk [14,42] to have the largest intrinsic hyperpolarizabilities. We anticipate that such chromophores will maintain large hyperpolarizabilities as the bridge is lengthened. If the weaker tendency to planarity becomes a problem, the χC region can be conformationally locked using synthetic strategies similar to the isophorone group in CLD (see Fig. 15). Given that even these small molecules were processable, it is likely that thin film devices can be fabricated using lengthened χC chromophores [43,44].

For supporting information, see 45.

Funding. National Science Foundation (NSF) (DMR-1303080, CHE-1212114); Air Force Office of Scientific Research (AFOSR) (FA9550-10-1-0558, FA9550-15-1-0319).

REFERENCES

1. P. Dong, Y.-K. Chen, G.-H. Duan, and D. T. Neilson, "Silicon photonic devices and integrated circuits," Nanophotonics **3**, 215–228 (2014).
2. E. Kuramochi, K. Nozaki, A. Shinya, K. Takeda, T. Sato, S. Matsuo, H. Taniyama, H. Sumikura, and M. Notomi, "Large-scale integration of wavelength-addressable all-optical memories on a photonic crystal chip," Nat. Photonics **8**, 474–481 (2014).
3. N. Kinsey, M. Ferrera, V. M. Shalaev, and A. Boltasseva, "Examining nanophotonics for integrated hybrid systems: a review of plasmonic interconnects and modulators using traditional and alternative materials [Invited]," J. Opt. Soc. Am. B **32**, 121–142 (2015).
4. W. Heni, C. Hoessbacher, C. Haffner, Y. Fedoryshyn, B. Baeuerle, A. Josten, D. Hillerkuss, Y. Salamin, R. Bonjour, A. Melikyan, M. Kohl, D. L. Elder, L. R. Dalton, C. Hafner, and J. Leuthold, "High speed plasmonic modulator array enabling dense optical interconnect solutions," Opt. Express **23**, 29746–29757 (2015).
5. C. Haffner, W. Heni, Y. Fedoryshyn, J. Niegemann, A. Melikyan, D. L. Elder, B. Baeuerle, Y. Salamin, A. Josten, U. Koch, C. Hoessbacher, F. Ducry, L. Juchli, A. Emboras, D. Hillerkuss, M. Kohl, L. R. Dalton, C. Hafner, and J. Leuthold, "All-plasmonic Mach–Zehnder modulator enabling optical high-speed communication at the microscale," Nat. Photonics **9**, 525–528 (2015).
6. J. L. Oudar and D. S. Chemla, "Hyperpolarizabilities of the nitroanilines and their relations to the excited state dipole moment," J. Chem. Phys. **66**, 2664–2668 (1977).
7. L. R. Dalton, P. A. Sullivan, D. H. Bale, and B. C. Olbricht, "Theory-inspired nano-engineering of photonic and electronic materials: Noncentrosymmetric charge-transfer electro-optic materials," Solid-State Electron. **51**, 1263–1277 (2007).
8. Y. Shi, C. Zhang, H. Zhang, J. H. Bechtel, L. R. Dalton, B. H. Robinson, and W. H. Steier, "Low (Sub-1-Volt) halfwave voltage polymeric electro-optic modulators achieved by controlling chromophore shape," Science **288**, 119–122 (2000).
9. P. A. Sullivan and L. R. Dalton, "Theory-inspired development of organic electro-optic materials," Acc. Chem. Res. **43**, 10–18 (2010).
10. C. Zhang, L. R. Dalton, M.-C. Oh, H. Zhang, and W. H. Steier, "Low Vπ electrooptic modulators from cld-1: chromophore design and synthesis, material processing, and characterization," Chem. Mater. **13**, 3043–3050 (2001).
11. C. H. Zhang, G. Todorova, C. Wang, T. Londergan, and L. R. Dalton, "Synthesis of new second-order nonlinear optical chromophores: implementing lessons learned from theory and experiment," Proc. SPIE **4114**, 77–87 (2000).
12. Y. Liao, C. A. Anderson, P. A. Sullivan, A. J. P. Akelaitis, B. H. Robinson, and L. R. Dalton, "Electro-optical properties of polymers containing alternating nonlinear optical chromophores and bulky spacers," Chem. Mater. **18**, 1062–1067 (2006).
13. L. R. Dalton, P. A. Sullivan, B. C. Olbricht, Y. Takimoto, J. J. Rehr, B. E. Eichinger, A. A. Mistry, D. Bale, H. Rommel, and B. H. Robinson, "Organic electro-optic/silicon photonic materials and devices," Proc. SPIE **6638**, 66380I (2007).
14. M. G. Kuzyk, J. Pérez-Moreno, and S. Shafei, "Sum rules and scaling in nonlinear optics," Phys. Rep. **529**, 297–398 (2013).
15. H. Kang, P. Zhu, Y. Yang, A. Facchetti, and T. J. Marks, "Self-assembled electrooptic thin films with remarkably blue-shifted optical absorption based on an X-shaped chromophore," J. Am. Chem. Soc. **126**, 15974–15975 (2004).
16. S. Keinan, E. Zojer, J.-L. Bredas, M. A. Ratner, and T. J. Marks, "Twisted π-system electro-optic chromophores. A CIS vs. MRD-CI theoretical investigation," J. Mol. Struct. THEOCHEM **633**, 227–235 (2003).
17. T. Kinnibrugh, S. Bhattacharjee, P. Sullivan, C. Isborn, B. H. Robinson, and B. E. Eichinger, "Influence of isomerization on nonlinear optical properties of molecules," J. Phys. Chem. B **110**, 13512–13522 (2006).

18. H. Kang, A. Facchetti, H. Jiang, E. Cariati, S. Righetto, R. Ugo, C. Zuccaccia, A. Macchioni, C. L. Stern, Z. Liu, S.-T. Ho, E. C. Brown, M. A. Ratner, and T. J. Marks, "Ultralarge hyperpolarizability twisted π-electron system electro-optic chromophores: synthesis, solid-state and solution-phase structural characteristics, electronic structures, linear and nonlinear optical properties, and computational studies," J. Am. Chem. Soc. **129**, 3267–3286 (2007).
19. M. H. van der Veen, M. T. Rispens, H. T. Jonkman, and J. C. Hummelen, "Molecules with linear π-conjugated pathways between all substituents: omniconjugation," Adv. Funct. Mater. **14**, 215–223 (2004).
20. R. R. Amaresh, D. Liu, T. Konovalova, M. V. Lakshmikantham, M. P. Cava, and L. D. Kispert, "Dendralene-type TTF vinylogs containing a 1, 3-diselenole ring," J. Org. Chem. **66**, 7757–7764 (2001).
21. M. R. Bryce, M. A. Coffin, P. J. Skabara, A. J. Moore, A. S. Batsanov, and J. A. K. Howard, "Functionalised oligoenes with unusual topologies: synthesis, electrochemistry and structural studies on redox-active [3]- and [4]-dendralenes," Chem. Eur. J. **6**, 1955–1962 (2000).
22. T. Michinobu, J. C. May, J. H. Lim, C. Boudon, J.-P. Gisselbrecht, P. Seiler, M. Gross, I. Biaggio, and F. Diederich, "A new class of organic donor–acceptor molecules with large third-order optical nonlinearities," Chem. Commun. **36**, 737–739 (2005).
23. J. C. May, J. H. Lim, I. Biaggio, N. N. P. Moonen, T. Michinobu, and F. Diederich, "Highly efficient third-order optical nonlinearities in donor-substituted cyanoethynylethene molecules," Opt. Lett. **30**, 3057–3059 (2005).
24. C. A. van Walree, V. E. M. Kaats-Richters, S. J. Veen, B. Wieczorek, J. H. van der Wiel, and B. C. van der Wiel, "Charge-transfer interactions in 4-donor 4′-acceptor substituted 1, 1-diphenylethenes," Eur. J. Org. Chem. **2004**, 3046–3056 (2004).
25. Cambridge Crystallographic Data Centre, https://summary.ccdc.cam.ac.uk/structure-summary-form.
26. C. Reichardt, "Solvatochromic dyes as solvent polarity indicators," Chem. Rev. **94**, 2319–2358 (1994).
27. J. P. Cerón-Carrasco, D. Jacquemin, C. Laurence, A. Planchat, C. Reichardt, and K. Sraïdi, "Solvent polarity scales: determination of new ET(30) values for 84 organic solvents," J. Phys. Org. Chem. **27**, 1099–1395 (2014).
28. D. P. Shelton, "Accurate hyper-Rayleigh scattering polarization measurements," Rev. Sci. Instrum. **82**, 113103 (2011).
29. P. Kaatz and D. P. Shelton, "Polarized hyper-Rayleigh light scattering measurements of nonlinear optical chromophores," J. Chem. Phys. **105**, 3918–3929 (1996).
30. M. G. Kuzyk, "Fundamental limits of all nonlinear-optical phenomena that are representable by a second-order nonlinear susceptibility," J. Chem. Phys. **125**, 154108 (2006).
31. M. J. Frisch, G. W. Trucks, H. B. Schlegel, G. E. Scuseria, M. A. Robb, J. R. Cheeseman, G. Scalmani, V. Barone, B. Mennucci, G. A. Petersson, H. Nakatsuji, M. Caricato, X. Li, H. P. Hratchian, A. F. Izmaylov, J. Bloino, G. Zheng, J. L. Sonnenberg, M. Hada, M. Ehara, K. Toyota, R. Fukuda, J. Hasegawa, M. Ishida, T. Nakajima, Y. Honda, O. Kitao, H. Nakai, T. Vreven, J. A. Montgomery, Jr., J. E. Peralta, F. Ogliaro, M. J. Bearpark, J. Heyd, E. N. Brothers, K. N. Kudin, V. N. Staroverov, R. Kobayashi, J. Normand, K. Raghavachari, A. P. Rendell, J. C. Burant, S. S. Iyengar, J. Tomasi, M. Cossi, N. Rega, N. J. Millam, M. Klene, J. E. Knox, J. B. Cross, V. Bakken, C. Adamo, J. Jaramillo, R. Gomperts, R. E. Stratmann, O. Yazyev, A. J. Austin, R. Cammi, C. Pomelli, J. W. Ochterski, R. L. Martin, K. Morokuma, V. G. Zakrzewski, G. A. Voth, P. Salvador, J. J. Dannenberg, S. Dapprich, A. D. Daniels, Ö. Farkas, J. B. Foresman, J. V. Ortiz, J. Cioslowski, and D. J. Fox, *Gaussian 09, Revision D.01* (Gaussian, Inc., 2009).
32. P. J. Stephens, F. J. Devlin, C. F. Chabalowski, and M. J. Frisch, "Ab initio calculation of vibrational absorption and circular dichroism spectra using density functional force fields," J. Phys. Chem. **98**, 11623–11627 (1994).
33. J. P. Perdew, M. Ernzerhof, and K. Burke, "Rationale for mixing exact exchange with density functional approximations," J. Chem. Phys. **105**, 9982–9985 (1996).
34. Y. Zhao and D. G. Truhlar, "Density functionals with broad applicability in chemistry," Acc. Chem. Res. **41**, 157–167 (2008).
35. T. Yanai, D. P. Tew, and N. C. Handy, "A new hybrid exchange-correlation functional using the Coulomb-attenuating method (CAM-B3LYP)," Chem. Phys. Lett. **393**, 51–57 (2004).
36. T. Kodaira, A. Watanabe, O. Ito, M. Matsuda, K. Clays, and A. Persoons, "Hyper-Rayleigh scattering studies of an ionic species Solvent effect on hyperpolarizability of 1-anilinonaphthalene-8-sulfonic acid ammonium salt," J. Chem. Soc. Faraday Trans. **93**, 3039–3044 (1997).
37. A. F. Tillack, L. E. Johnson, M. Rawal, L. R. Dalton, and B. H. Robinson, "Modeling chromophore order: a guide for improving EO performance," in *Symposium II/JJ/KK: Materials, Processes and Devices for Nanophotonics, Nonlinear Optics and Resonant Optics* (2014), Vol. **1698**
38. A. F. Tillack, L. E. Johnson, B. E. Eichinger, and B. H. Robinson, "Systematic generation of anisotropic coarse-grained Lennard-Jones potentials and their application to ordered soft matter," J. Chem. Theory Comput. **12**, 4362–4374 (2016).
39. S. J. Cyvin, J. E. Rauch, and J. C. Decius, "Theory of hyper-raman effects (nonlinear inelastic light scattering): selection rules and depolarization ratios for the second-order polarizability," J. Chem. Phys. **43**, 4083–4095 (1965).
40. K. Tripathy, J. P. Moreno, M. G. Kuzyk, B. J. Coe, K. Clays, and A. M. Kelley, "Why hyperpolarizabilities fall short of the fundamental quantum limits," J. Chem. Phys. **121**, 7932–7945 (2004).
41. A. F. Tillack and B. H. Robinson, "Toward optimal EO response from ONLO chromophores: a statistical mechanics study of optimizing shape," J. Opt. Soc. Am. B **33**, E121–E129 (2016).
42. R. Lytel, S. Shafei, and M. G. Kuzyk, "Nonlinear optics of quantum graphs," Proc. SPIE **8474**, 847400 (2012).
43. M. Rawal, K. Garrett, A. F. Tillack, W. Kaminsky, E. Jucov, D. P. Shelton, T. V. Timofeeva, B. E. Eichinger, B. H. Robinson, and L. R. Dalton, "Cross-conjugation as a motif for organic non-linear optical molecules," in *Symposium II/JJ/KK: Materials, Processes and Devices for Nanophotonics, Nonlinear Optics and Resonant Optics* (2014), Vol. **1698**
44. M. Rawal, *Cross-Conjugated Moieties as Design Motifs for a Class of Novel Electro-Optic Chromophores* (University of Washington, 2013).
45. https://www.dropbox.com/s/9xxz7bmftj661m0/XC%20Supp%20Info%20v15.pdf?dl=0.